Spectroscopic determination of final products of autoionization

W. E. Cooke and S. A. Bhatti
Department of Physics, University of Southern California, Los Angeles, California 90007
(Received 19 May 1980; revised manuscript received 4 September 1981)

A detailed analysis of the excitation spectrum of the Ba ($6P_{3/2}12s$, $J=1$) autoionizing state is presented. From this it is deduced that the dominant decay channel for autoionization of the Ba ($6P_{3/2}ns$, $J=1$) states ($n \geq 12$) is to the Ba^+ ($6P_{1/2}$)$+e^-\epsilon d$ configuration. Quadrupole coupling is presumed to be the important interaction, and an estimate of the resulting autoionization rate is presented.

I. INTRODUCTION

All but the lowest few doubly excited states of Ba have energies greater than the ionization limit and thus autoionize into a Ba^+ ion and a free electron. There are typically several possible final states of the ion [e.g., Ba^+ ($6S$) or Ba^+ ($5D_j$)] since the electron can carry away an arbitrary amount of kinetic energy. In a recent study[1] of the $6P_j20s$ states of Ba, it was postulated that the barium in the $6P_{3/2}20s$, $J=1$ state autoionized primarily into optically excited ions, Ba^+ ($6P_{1/2}$). Since then, this has been verified by an energy analysis of the electrons emitted during autoionization.[2] However, even this does not present a complete picture of the process, since the electrons may be emitted as either s or d partial waves and still conserve parity and angular momentum. The $6P_{3/2}20s$, $J=2$ state is not allowed to autoionize into a Ba^+ ($6P_{1/2}$) and s-wave electron due to angular momentum considerations and since it does autoionize much more slowly than the $J=1$ state, it was initially assumed that the electrons from the $J=1$ state were emitted as s waves. The autoionization mechanism was thus thought to be either a spin-spin or a spin-other orbit interaction.[1]

The spectroscopic data reported in this work, and their accompanying analysis strongly suggest that the electrons are in fact emitted as d waves and that the important interaction is electrostatic. We base this conclusion on an analysis of the excitation spectrum of the barium transition, $6s\,12s\ ^1S_0 \rightarrow 6P_{3/2}12s$, $J=1$. As shown in Fig. 1, the $6P_{3/2}12s$ state lies below the Ba^+ ($6P_{1/2}$)$+e^-$ ionization limit, and thus it cannot autoionize into a Ba^+ ($6P_{1/2}$) ion. (It does, however, autoionize into Ba^+ ions in the $6S$ and $5D_j$ states.) The interaction which causes autoionization of the higher states ($n>12$) into Ba^+ ($6P_{1/2}$) ions is nevertheless present and results in a distortion of the $6s\,12s\ ^1S_0 \rightarrow 6P_{3/2}12s$, $J=1$ excitation profile at the location of the $6P_{1/2}nl$ doubly excited states. For $6P_{1/2}nl$ states within the $6P_{3/2}12s$ autoionization-broadened linewidth, one sees relative minima in the excitation line shape. For states far from the $6P_{3/2}12s$ state, one sees relative maxima. By noting the locations of the major distortions, we have identified the $6P_{1/2}nd$ states as being more strongly coupled to the $6P_{3/2}12s$ state than the $6P_{1/2}ns$ states. For $n>12$, then, a $6P_{3/2}ns$ state presumably autoionizes primarily into the Ba^+ ($6P_{1/2}$) $+e^-(\epsilon d)$ continuum.

This technique should be applicable to many autoionizing states and should thus provide a general method for determining autoionization-branching ratios. Since it is a purely spectroscopic technique, it avoids all the difficulties inherent in collecting and analyzing emitted electrons without distorting their emission pattern. It does, however, have its

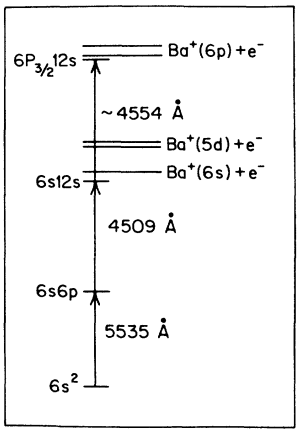

FIG. 1. Energy level diagram for excitation of the $6P_{3/2}12s$ state of Ba. The five lowest ionization limits of Ba are designated.

own difficulties associated with the analysis of a complex spectrum.

II. EXPERIMENTAL METHOD

An excitation spectrum was obtained by first exciting barium atoms, stepwise, from the $6s^2$ state via the $6s\,6p\ ^1P_1$ state to the $6s\,12s\ ^1S_0$ state ($E = 40233.74\ \text{cm}^{-1}$, see Ref. 3) as shown in Fig. 1. Then a third laser was tuned about the Ba^+ $6S \rightarrow 6P_{3/2}$ ion resonance (4554 Å) and the total number of resulting ions was recorded. Since the autoionization rates of all states in this region are much greater than the radiative decay rates, the number of ions is the same as the number of atoms excited from the $6s\,12s\ ^1S_0$ state. The procedure and apparatus was very similar to that used in Ref. 1.

The source of Ba atoms was an effusive atomic beam which was directed to a region between two electric field plates, where it was crossed by the three laser beams. The top plate had a grid in it, and the bottom plate was pulsed after each laser shot to drive Ba^+ ions through the grid, into an EMI, venetian blind electron multiplier. The pulses of ions were integrated by a PAR 162 boxcar averager and recorded on a chart recorder.

The lasers were Hansch-type dye lasers, using grazing incidence prisms as beam expanders. They were pumped by the second or third harmonics of a Quanta-Ray Nd:YAG laser. Typical dye laser characteristics were 2-kW pulses with 0.2-cm^{-1} linewidth.

The wavelength of the third laser ($\sim$4554 Å) was calibrated using a marker resonance[3] at 21 938.1 cm^{-1} corresponding to the transitions:

$$6s\,6p\ ^1P_1 \rightarrow 6s\,10d\ ^1D_2 \rightarrow 6P_{3/2}\,10d \rightarrow Ba^+ + e^- \,. \tag{1}$$

This results in a large narrow peak, the amplitude of which varies as the square of the third-laser intensity. The scan rate of the third laser was measured by monitoring the power transmitted through a 1.68-cm^{-1} free spectral range etalon. This produced wavelength measurements accurate to better than 0.5 cm^{-1}; however, the laser scan rate typically exhibited nonlinearities as large as 5%.

Figure 2 shows typical data over the wavelength range 4545–4590 Å. The large feature at 4558 Å is the "marker" transition. The wavelengths shown in the figure are only approximate since they represent a linear wavelength scale.

III. ANALYSIS

This technique of optically exciting an ionic core after "removing" a valence electron by exciting it to a Rydberg state, is useful because of the simplicity it introduces into the excitation of autoionizing states.[1] Usually only one state of a well-known configuration is excited because the only large transition moment corresponds to a core excitation with no change in the Rydberg electron's state. Configuration mixing is nevertheless important in these doubly excited states, as it is what leads to

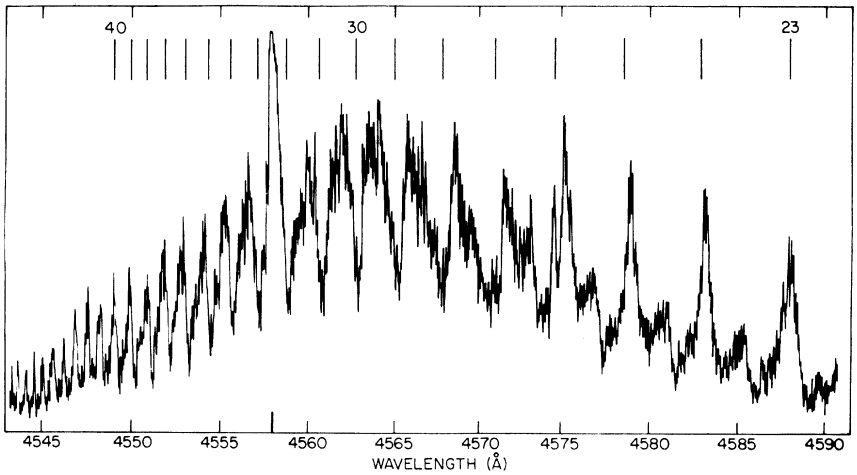

FIG. 2. Photoionization spectrum from Ba ($6s\,12s\ ^1S_0$). The vertical lines at the top of the figure designate the positions of the $6P_{1/2}nd$ states for values of $n = 23$ to 40. The $6P_{1/2}ns$ states are located almost exactly midway between $6P_{1/2}nd$ states.

their autoionization by coupling the states to different core configurations. Thus, for example, a Ba $6P_{3/2}ns$, $J=1$ state is coupled to a Ba^+ $(6P_{1/2})+e^1(\epsilon l)$ configuration (where ϵ and l refer to the electron's energy and angular momentum, respectively). This coupling shows up most dramatically as autoionization for $n \geq 13$, but even for $n=12$ the coupling still exists. (Since the interaction occurs in the vicinity of the core, it is insensitive to the Rydberg electron's binding energy which is small compared to its total kinetic energy when it is near the core.) The configuration interaction shows up in this case as structure in the $6s\,12s \rightarrow 6P_{3/2}12s$ excitation profile, since $6P_{1/2}nl$ states of many values of n $(24 < n^* < 35)$ lie within the autoionization-broadened $6P_{3/2}12s$ state linewidth, as shown in Fig. 3. (Safinya and Gallagher[4] have recently seen a similar excitation spectrum modification due to other Rydberg states with the same core configuration.)

To model the excitation spectrum we first distributed the $6P_{3/2}12s$ wave function over a band of energy represented by a Lorentzian of FWHM Γ_0 and line center E_0, thus constructing a "continuum" wave function which is normalized per unit energy and depends both on position and energy as

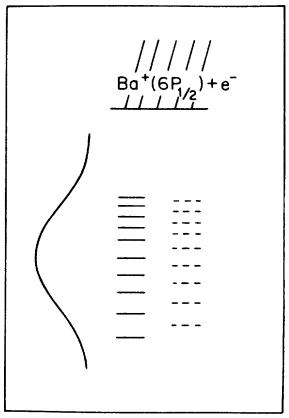

FIG. 3. Expanded view of states in the vicinity of the Ba $(6P_{3/2}12s)$ state. The broad feature represents the $6P_{3/2}12s$ state which is broadened to an 85-cm^{-1} linewidth by autoionization which occurs rapidly for low n states. The solid lines represent $6P_{1/2}nd$ states; the dashed lines represent $6P_{1/2}ns$ states. For both cases $n \simeq 30$, and thus their autoionization linewidth is small, ~ 2 cm^{-1}. Configuration interaction results in structure (not shown) in the excitation line shape of the $6P_{3/2}12s$ state. The location of this structure determines whether the state mixes primarily with the $6P_{1/2}nd$ configuration or the $6P_{1/2}ns$ configuration.

follows:

$$q \equiv 2(E-E_0)/\Gamma_0 \,, \tag{2a}$$

$$|\,6P_{3/2}Es\,\rangle = \left[\frac{2}{\pi\Gamma_0}\frac{1}{1+q^2}\right]^{1/2} |\,6P_{3/2}12s\,\rangle \,. \tag{2b}$$

We next applied an approximation of the Fano formalism,[5–7] since this spectrum involved many bound states and two-continuum channels. Here we have modeled the $6P_{1/2}nl$ states as bound states and the ionization channels are (a) the constructed $6P_{3/2}Es$ continuum and (b) the other Ba^+6S and $5D$ channels grouped together. The (a) channel is illustrated in Fig. 3 where many of the $6P_{1/2}nl$ states (dashed and solid horizontal lines) can "autoionize" by making a transition to the broad $6P_{3/2}12s$ state. The (b) channels are evident in Fig. 1, where it is shown that any states near the $6P_{3/2}12s$ state are in the continuum, being above the $6S$ and $5D$ ionization limits.

It is easier to understand the character of the spectrum in the case where all of the broadening of the $6P_{1/2}nl$ state is due to transitions to the broad $6P_{3/2}12s$ state. Then the strength of the bound-continuum interaction has a simple form:

$$V_{nE} \equiv \left[\frac{2}{\pi\Gamma_0}\frac{1}{(1+q^2)}\right]^{1/2} \langle\, 6P_{1/2}nl\,|\,1/r_{12}\,|\,6P_{3/2}12s\,\rangle \,, \tag{3a}$$

$$\Gamma_1 \equiv 2\pi(n^*)^3\,|\,\langle\, 6P_{1/2}nl\,|\,1/r_{12}\,|\,6P_{3/2}12s\,\rangle\,|^2 \,, \tag{3b}$$

$$\pi\,|\,V_{nE}\,|^2 = \frac{\Gamma_1}{\Gamma_0}\frac{1}{\pi(n^*)^3}\frac{1}{(1+q^2)} \,, \tag{3c}$$

where n^* is the effective quantum number of states $6P_{1/2}nl$, such that its binding energy $E_n = -1/(2n^{*2})$ (a.u.) relative to the Ba^+ $(6P_{1/2})+e^-$ ionization limit, and the additional factor in (3a) represents the distribution of the $6P_{3/2}12s$ wave function over the energy band Γ_0. Γ_1 represents the autoionization rate that would exist for Ba $(6P_{3/2}12s) \rightarrow Ba^+$ $(6P_{1/2})$ $+e^-(\epsilon l)$ if that channel had been open. Γ_1 is obtained by scaling the appropriate rate for Ba $(6P_{3/2}ns)$ states with $n > 12$.

Using Fano's formalism, this interaction causes a $6P_{1/2}nl$ state to have an admixture of the broad $6P_{3/2}12s$ state:

$$|6P_{1/2}nl\rangle + P\int \frac{V_{E'n}}{E'-E_n}|6P_{3/2}E's\rangle dE' = |6P_{1/2}nl\rangle + \frac{q}{1+q^2}\left[\frac{2\Gamma_1}{\pi\Gamma_0^2(n^*)^3}\right]^{1/2}|6P_{3/2}12s\rangle . \quad (4)$$

If the transition moment from the $6s\,12s$ state to the "bound" state $6P_{1/2}nl$ is much smaller than the transition moment to the "continuum" state $6P_{3/2}12s$, then the q defined in Eq. (2a) is identical to the Fano q. The Fano q is proportional to the transition moment to the $|6P_{1/2}nl\rangle$ state (including its admixture of $6P_{3/2}12s$) divided by the transition moment to the portion of $|6P_{3/2}Es\rangle$ state lying within the energy band $\pi|V_{nE}|^2$. For our case, transition moments due to the $6P_{1/2}nl$ character will be smaller than those due to $6P_{3/2}12s$ character by a factor of the order of $n^{*-1.5}$ whether due to Rydberg electron wave function overlap (e.g., $|\langle ns|12s\rangle|$) or due to excitation from a mixed configuration (e.g., $|\langle 6p^2|r|6pns\rangle| \simeq 1/n^{*1.5}$). The spectrum then consists of a series of Beutler-Fano profiles such that $|q|$ increases according to Eq. (2a) for energies farther from E_0, while the fractional linewidth (the ratio of the linewidth to the interstate spacing, n^{*-3}) decreases as a Lorentzian of peak value $2\Gamma_1/\pi\Gamma_0$. The maximum amplitude of each of these features attains the same value; however, since the width of the features decreases, the averaged excitation strength follows the original Lorentzian profile. It should be noted that, because of the variation of q, the perturbing states n are located near minima at $E_n \simeq E_0$, but near maxima for $|E_n - E_0| > \Gamma_0$.

It should also be noted that this approach gives results qualitatively similar to those that the multichannel quantum-defect theory (MQDT) would give if both the $6P_{3/2}12s$ and $6P_{1/2}nl$ states were treated as channels. We chose not to treat the problem this way because the width of the $6P_{3/2}12s$ state, excluding coupling to the $6P_{1/2}nl$ states, is expected to be greater than the $6P_{1/2}nl$ interstate spacing (as in Fig. 3). In such a case it is impossible for the channels to show the dramatic quantum-defect shifts which were first used to justify MQDT. Moreover, a complete MQDT treatment would require knowledge of all possible interacting channels (at least eight open channels and four or more closed channels) since partial MQDT analyses have not shown exceptional accuracy.[8]

Now, when the additional broadening is introduced [i.e., when we allow the $6P_{1/2}nl$ states to also autoionize to the $Ba^+(6s)$ and $Ba^+(5d)$ channels] then the spectra are averaged since this prevents the width of the features from decreasing indefinitely. By broadening each feature in a manner similar to that done by Fano for the single-bound-state—two-continuum case,[5] we obtained for the spectra, $I(E)$:

$$I(E) = \frac{(qZ-1)^2}{(1+Z^2)(1+q^2)[\Gamma_1/\Gamma_0 + (1+q^2)(\frac{1}{2}\pi\Gamma_0\nu^3)]}, \quad (5a)$$

$$Z(E) = \frac{1}{\pi}\sum_n \frac{(\frac{1}{2}\pi\Gamma_0\nu^3) + (\Gamma_1/\Gamma_0)/(1+q^2)}{n^{*3}(E-E_n)}, \quad (5b)$$

where ν is the effective quantum number of the $6P_{3/2}12s$ state (relative to the $6P_{3/2}$ ionization limit), and $E_n = -1/2(n^*)^2 = -1/2(n-\delta)^2$, for the $6P_{1/2}nl$ states having quantum defect δ. For simplicity, we have again used Γ_0, scaled by $(n^*)^{-3}$, as the autoionization width of the $6P_{1/2}nl$ channels due to the additional channels.

Equation (5) can be obtained from Ref. 5 by making the correspondence between Z and $-\tan\Delta$ of Eq. (60) in Ref. 5, extended to the two-continuum case using Eq. (41) of Ref. 5. Thus, the first term in the numerator of the expression for Z represents coupling to the additional ($6S^+$ and $5D^+$) channels, and the second term represents the $\pi|V_{nE}|^2$ coupling of Eq. (3c). The signal I has three factors: the first represents the reduced coupling since the two-continuum problem has two independent solutions, only one of which shows interference effects. In Ref. 5, this effect is the first factor of Eq. (40b). The second factor of Eq. (5b) is due to the overall envelope of the $|6P_{3/2}Es\rangle$ constructed continuum as defined in Eq. (2b). The third factor represents the basic interference and occurs in Ref. 5 as $\cos^2\Delta(q\tan\Delta - 1)^2$.

The longer wavelength wing of the data in Fig. 2 clearly shows two series of $6P_{1/2}nl$ peaks, with one set approximately three times as large as the other. Since these features are far from line center, the peaks should be located very near the energy of $6P_{1/2}nl$ states. In fact, the large features are very

near $6P_{1/2}nd$ states, and the smaller features are near $6P_{1/2}ns$ states. In Fig. 2, the lines at the top of the figure correspond to the location of the $6P_{1/2}nd$ states. The $6P_{1/2}ns$ states are located almost exactly ($\pm 10\%$) midway between those lines.[6]

To characterize the structure near line center, we created a spectrum according to Eq. 5; however, we only assumed coupling to the $6P_{1/2}nd$ states. To determine Γ_0 and Γ_1, we used the linewidth data of the $6P_j20s$ states which suggested that the $6P_{3/2}20s$ state had an autoionization linewidth of $0.05(n^*)^{-3}$ (a.u.) due to coupling to the $6s$ and $5d$ ion channels, and $0.09(n^*)^{-3}$ due to coupling to the $6P_{1/2}$ ion channels. For Γ_0, we used the sum of the $6s$ and $5d$ contribution (25 cm^{-1}) and one-fourth of the other contribution (15 cm^{-1}), representing coupling to the unused $6P_{3/2}ns$ channels. Thus, our parameters were $\Gamma_0=40$ cm^{-1}, $\Gamma_1=45$ cm^{-1}, $E_0=62150$ cm^{-1} (corresponding to $\upsilon=7.73$, extrapolated from higher $6P_{3/2}ns$ states), and $\delta=2.73$ (as observed for $6P_{1/2}nd$ states).

Figure 4 shows the comparison between data and computer prediction (solid line) over the wavelength range 4550–4575 Å. The agreement is substantial in many aspects (e.g., feature position and assymmetry), thus implying that for $n>12$, $J=1$, the dominant autoionization channel produces a d-wave electron:

$$\text{Ba}\,(6P_{3/2}ns)\rightarrow \text{Ba}^+\,(6P_{1/2})+e^-(\epsilon d)\ . \qquad (6)$$

IV. DISCUSSION

In order to judge the comparison of the data to the model, one must consider the approximations made and the resulting limitations of the model. Equation (2b) distributes the $6P_{3/2}12s$ wave functions over a Lorentzian line shape. An MQDT analysis of the $6P_{3/2}ns$ states would result in two major changes in this aspect of the model. First, since other terms in the $6P_{3/2}ns$ channel interact in a similar fashion, one should sum over all n values. However, to the extent that these states can also be modeled as Lorentzians (a reasonable approximation for two channel MQDT), the contributions of the nearest neighbors would be down by an order of magnitude at 20-Å detuning from the $6P_{3/2}12s$ resonance. The second, related, aspect is that the spatial behavior of an MQDT wave function changes with energy to reflect the change in the Rydberg electrons binding energy. Near line center this typically results in a modification of matrix elements by the factor[9] $\sin^2(\pi\Delta n^*)/(\pi\Delta n^*)^2$ where Δn^* is the change in effective quantum number from line center. For 20-Å detuning in our case, this factor causes a 20% decrease, which should primarily result in a discrepancy in feature linewidths.

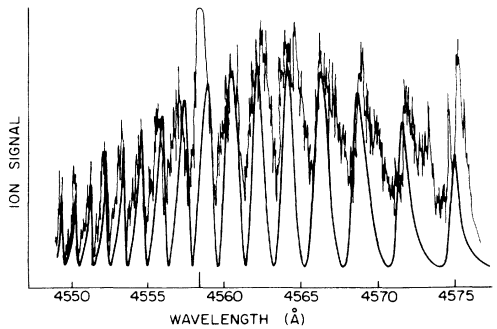

FIG. 4. Comparison of calculated spectrum vs observed spectrum assuming coupling of $6P_{3/2}12s$, $J=1$ state to $6P_{1/2}nd$ states. Wavelength is vacuum wavelength. The large peak near 4558 Å is a frequency marker.

The other major approximation made was the assumption that the $6P_{1/2}nl$ states were properly diagonalized. As MQDT shows, the orthogonality of $6P_{1/2}nl$ states and their diagonalization results from a complex interplay between the satisfaction of boundary conditions and the variation of Rydberg wave functions with energy. Thus, if one Rydberg state is perturbed, it is no longer orthogonal to other unperturbed states. The square of the overlap between adjacent Rydberg states is again $\sin^2\pi(n_2^*-n_1^*)$, which will have little effect on our model, except for when states are broadened sufficiently that $n_2^*-n_1^*$ differs appreciably from an integer.

Neither of the assumptions mentioned above appreciably affect the positions of the features relative to the "true" position of the $6P_{1/2}nl$ states, which can be determined by excitation directly from the $6snl$ Rydberg states.[1,6] And, as mentioned earlier, the minima near the center of the profile, and the maxima in the wings are located near the energies of the admixed $6P_{1/2}nl$ states. Since these energies are determined separately, this conveniently allows a spectrum comparison that is relatively insensitive to the $6P_{3/2}12s$ state width Γ_0, the mixing parameter Γ_1, and the model's limitations. Thus it is possible to claim dominance of the $6P_{1/2}nd$ channel, even though the spectrum comparison does show discrepancies.

There are two major discrepancies between the

predicted and actual spectrum shown in Fig. 4. We attribute both to shortcomings in our model. Most notable is the failure to reproduce the extra features which we ascribe to mixing with the $6P_{1/2}ns$ configuration. The feature at 4573 Å appears as a shoulder, while at 4585 Å (Fig. 2) a similar feature has evolved into a discrete peak. Our first attempts at including the $6P_{1/2}ns$ configuration successfully generated peaks in the wings, but badly reduced the agreement at line center by introducing additional minima. Further attempts at modeling the two-configuration, two-continuum problem are continuing.

The second discrepancy is between the predicted and actual feature widths near the spectrum's center. Part of this may be due to the omission of the $6P_{1/2}ns$ configuration, but we believe part of it is also due to an overestimating of the coupling, V_{nE}. For features near the center, Eq. (3b) predicts an "autoionization" linewidth larger than the spacing between states. In the spectrum this means the central peaks correspond to narrow spaces between broad minima. Physically, this is unlikely as it represents an "autoionization" lifetime shorter than the orbit period. We believe the approximate solutions are failing because this strong coupling would produce large, higher-order couplings between adjacent $6P_{1/2}nd$ states as described above. A proper treatment using a modified MQDT would probably show a reduced coupling V_{nE} (typically MQDT departs from perturbation theory when couplings are large, and always results in a smaller net effect).

Since the $6P_{3/2}ns$ states ($n > 12$) autoionize to the $6P_{1/2}\epsilon d$ channel, we believe that the quadrupole term of the expansion of $1/r_{12}$ is responsible (where r_{12} is the distance between the core and Rydberg electrons). This autoionization mechanism is completely general and does not depend on ionic fine structure, or various spin couplings as initially[1] believed. However, as reported earlier,[1] the $6P_{3/2}20s$, $J=1$ and $J=2$ states have considerably different autoionizing rates; this suggests that the coupling is primarily through the singlet character of the states (since the $J=2$ state has pure $^3P_2$ character). It is not unusual for those interactions which are sizable only near the core to be larger for singlet states since they have greater electron spatial wave function overlap. Accordingly, we have made the following estimation:

$$\left\langle 6P_{3/2}ns \left| \frac{1}{r_{12}} \right| 6P_{1/2}\epsilon d \right\rangle \simeq (n^*)^{3/2}\left(\tfrac{2}{15}\right)\langle 6P \mid r_1^2 \mid 6P\rangle \left\langle ns \left| \frac{1}{r_2^3} \right| nd \right\rangle \simeq \frac{5.7}{l(l+\frac{1}{2})(l+1)}(n^*)^{-3/2}, \tag{7}$$

where $\frac{2}{15}$ is due to geometric factors, and the matrix elements are estimated from hydrogenic scaling[10] using the diagonal $l=2$ case for the Rydberg matrix element. From Eq. (7) we obtained a mixing parameter Γ_1, for the $6P_{3/2}12s$ state of 200 cm^{-1} to be compared to the 45 cm^{-1} used here; a reasonable agreement considering the approximations certainly produce an overestimation (because of the use of the diagonal Rydberg matrix element and because the electrostatic expansion is not valid for $r_2 < r_1$).

V. CONCLUSION

The measurement reported here presents an alternate method for determining the branching ratio of autoionization into different (energy degenerate) partial waves. Since the method is purely spectroscopic, it does not have any of the difficulties usually encountered when measuring the energy and direction of electrons. Although a complete analysis is difficult, the location of dominant features will often designate the primary autoionization channel. For the case of Ba ($6P_{3/2}$, ns) $J=1$, $n > 12$ states, this analysis shows that the primary autoionization route results in d-wave electrons.

ACKNOWLEDGMENTS

This work was supported by a Cottrell Research Grant from the Research Corporation. Partial support was provided by the NSF under Grant No. PHY79-16444. We would like to acknowledge useful discussions with T. F. Gallagher and W. Sandner.

[1]W. E. Cooke and T. F. Gallagher, Phys. Rev. Lett. 41, 1648 (1978).
[2]T. F. Gallagher, K. A. Safinya, and W. E. Cooke, Phys. Rev. A 21, 148 (1980).
[3]J. R. Rubbmark, S. A. Börgstrom, and K. Bockasten, J. Phys. B 10, 421 (1977).
[4]K. A. Safinya and T. F. Gallagher, Phys. Rev. Lett. 43, 1239 (1979).
[5]U. Fano, Phys. Rev. 124, 1866 (1961).
[6]W. E. Cooke, S. A. Bhatti, and T. F. Gallagher (unpublished). See also C. M. Brown and M. L. Ginter, J. Opt. Soc. Am. 68, 817 (1978), in which the energies of the $6P_j ns$ states can be deduced from absorption minima, since the lines are low q.
[7]K. T. Lu, Phys. Rev. A 4, 579 (1972).
[8]C. F. Fischer and J. E. Hansen, Phys. Rev. A 24, 631 (1981).
[9]S. A. Bhatti, C. L. Cromer, and W. E. Cooke, Phys. Rev. A 24, 161 (1981).
[10]E. U. Condon and G. H. Shortley, *The Theory of Atomic Spectra* (Cambridge University Press, Oxford, 1935).